# Entanglement of magnetically levitated massive Schrödinger cat states by induced dipole interaction

Ryan J. Marshman [1] Sougato Bose,[2] Andrew Geraci,[3] and Anupam Mazumdar[4]

[1]*Centre for Quantum Computation and Communication Technology, School of Mathematics and Physics,*
*University of Queensland, Brisbane, Queensland 4072, Australia*
[2]*Department of Physics and Astronomy, University College London, Gower Street, WC1E 6BT London, United Kingdom*
[3]*Center for Fundamental Physics, Department of Physics and Astronomy, Northwestern University, Evanston, Illinois 60208, USA*
[4]*Van Swinderen Institute, University of Groningen, 9747 AG Groningen, The Netherlands*

Quantum entanglement provides a novel way to test short-distance quantum physics in a nonrelativistic regime. We provide entanglement-based protocols to potentially test the magnetically induced dipole-dipole interaction and the Casimir-Polder potential between the two nanocrystals kept in a Schrödinger cat state. Our scheme is based on the Stern-Gerlach (SG) apparatus, where we can witness the entanglement mediated by these interactions for the nanocrystal mass $m \sim 10^{-19}$ kg with a spatial superposition size of order 0.1 μm in a trap relying on diamagnetic levitation. We show that it is possible to close the SG interferometer in position and momentum with a modest gradient in the magnetic field.

Quantum entanglement is a critical observable that demarcates the classical from the quantum world [1]. Entanglement provides a quantum signature that cannot be mimicked by any classical operation between two quantum systems. The theorem local operation and classical communication (LOCC) prohibits entanglement formation between two quantum systems using only classical interactions [2]. The standard model (SM) interactions are known to be quantum, and quantum entanglement-based protocols allow us to test this in a laboratory setup [3]. At short distances, but still in the infrared (IR) regime, we can test virtual photon-induced interactions [4], such as Coulomb, Casimir-Polder [5], and magnetically induced dipole-dipole interactions [6].

Gravitationally mediated entanglement has been proposed as a key protocol to test the quantum nature of gravity in the laboratory [7–9]). The scheme relies on two masses, each prepared in a spatial superposition and placed such that they couple solely gravitationally. If gravity is a quantum interaction, and a classical-valued field, then the two masses will entangle [8,10–14]. This requires heavy masses, $10^{-14}$–$10^{-15}$ kg, large spatial superposition, 10–100 μm, and long coherence times, 1–2 s. One can also test the quantum origin of the gravitational interaction between quantum matter and light [15], which will enable us to understand the spin nature of the gravitational interaction. These protocols are commonly known as quantum gravity-induced entanglement of masses (QGEM) [8]. One crucial ingredient for these experiments is to understand the entanglement generation from the known photon-induced electromagnetic interactions. The photon-induced entanglement will create a background which must be characterized before we could perform the QGEM experiment [4,16].

The aim of this Letter will be to present a method of doing this characterization with neutral nanocrystals in the presence of an external magnetic field. The external magnetic field, which is required for trapping the nanocrystal, and creating the quantum superposition, will induce a magnetic dipole to the nanocrystal. The two nanocrystals in a quantum superposition will entangle through their electromagnetic interactions.

The use of a Stern-Gerlach (SG) apparatus is one of the most promising approaches toward atomic and larger-scale particle interferometry [17–27]. Such interferometers have been realized using atom chips [19], for both half-loop [18] and full-loop [20] configurations achieving a superposition size of 3.93 and 0.38 μm in 21.45 and 7 ms, respectively. Based on this SG scheme there have been studies to create even more ambitious superposition sizes [25–27]. In all cases, the idea is to manipulate the nitrogen vacancy (NV) center of a nanodiamond. The NV center provides a spin defect, which interacts with an external magnetic field. One can then use these spins to witness the entanglement through spin correlations [8,28].

One of the key challenges is to understand the numerous sources of decoherence and noise [4,8,29–35]. They arise from residual gas collisions and environmental photons, which can be attenuated by vacuum and low temperatures [36,37]. In addition, the Humpty-Dumpty effect [38], internal cooling of the nanodiamond to improve the spin coherence time [39–42], as well as to tackle the Majorana spin flip, is under development [24]. There are also a series of gravitational channels for dephasing [35,43]; the emission of gravitons is negligible [44], gravity gradient noise (GGN) can be mitigated with an exclusion zone [35], and relative acceleration can be mitigated by improving the vacuum and isolating the experiment.

In this Letter we propose a method for understating two particular Electro-Magnetic (EM)-induced potentials which will feature in future large mass entanglement experiments. These will form an important consideration for future devices even when the monopole contribution is neutralized, as is experimentally feasible [45]. The two potentials are the Casimir-Polder (CP) potential and the induced dipole-dipole

(DD) potential due to the presence of an external magnetic field. We will provide a superposition scheme in a levitating setup to witness the entanglements due to these potentials. We will show that with modest magnetic field gradients in the SG setup, we can measure the entanglement witness for both CP and DD potentials for a $m \sim 10^{-19}$ kg neutral nanodiamond and a 0.1 μm spatial superposition.

A diamagnetic material in a magnetic trapping potential will evolve according to the Hamiltonian

$$\hat{H} = \frac{\hat{\mathbf{p}}^2}{2m} + \hbar D \hat{S}_z + g_s \frac{e\hbar}{2m_e} \hat{\mathbf{S}} \cdot \mathbf{B} + mg\hat{y} - \frac{\chi_\rho m}{2\mu_0} \mathbf{B}^2, \quad (1)$$

where $\hat{\mathbf{p}}$ is the momentum operator and $m$ is the mass of the nanodiamond. The second term represents the zero-field

splitting of the NV center with $D = (2\pi) \times 2.8$ GHz, $\hbar$ is the reduced Planck constant, and $\hat{S}_z$ is the NV axis aligned spin component operator. The third term represents the interaction energy of the NV electron spin magnetic moment with the magnetic field **B**. The spin magnetic moment operator $\hat{\boldsymbol{\mu}} = -g_s \mu_B \hat{\mathbf{S}}$, where $g_s \approx 2$ is the Landé $g$ factor, $\mu_B = e\hbar/2m_e$ is the Bohr magneton, and $\hat{\mathbf{S}}$ is the NV spin operator. The fourth term is the gravitational potential energy, $g \approx 9.8$ m/s$^2$ is the gravitational acceleration, and $\hat{z}$ is the position operator along the direction of gravity ($z$ axis). The final term represents the magnetic energy of a diamagnetic material in a magnetic field, $\chi_\rho = -6.2 \times 10^{-9}$ m$^3$/kg is the mass susceptibility, and $\mu_0$ is the vacuum permeability.

For our scheme, we will make use of a trap profile $\mathbf{B}_T$ given by [46]

$$\mathbf{B}_T = -\left[ \frac{3a_4\sqrt{\frac{35}{\pi}}x^2 y}{8y_0^3} + \frac{3a_4\sqrt{\frac{35}{\pi}}y(x^2-y^2)}{16y_0^3} - \frac{a_3\sqrt{\frac{7}{6\pi}}x^2}{y_0^2} + \frac{a_2\sqrt{\frac{15}{\pi}}y}{4y_0} + \frac{a_3\sqrt{\frac{7}{6\pi}}(-x^2-y^2+4z^2)}{2y_0^2} \right]\hat{x}$$

$$- \left[ -\frac{3a_4\sqrt{\frac{35}{\pi}}xy^2}{8y_0^3} + \frac{3a_4\sqrt{\frac{35}{\pi}}x(x^2-y^2)}{16y_0^3} - \frac{a_3\sqrt{\frac{7}{6\pi}}xy}{y_0^2} + \frac{a_2\sqrt{\frac{15}{\pi}}x}{4y_0} \right]\hat{y} - \left[ \frac{2a_3\sqrt{\frac{14}{3\pi}}xz}{y_0^2} \right]\hat{z} \quad (2)$$

where $y_0 = 75$ μm is the distance from the center of the trap to the pole pieces which help generate the trap and $a_2 = -1.3$ T, $a_3 = 0.0183$ T, and $a_4 = 0.72$ T determine the magnetic field strength. We will take the particle at time $t = 0$ to be at rest in the trapping potential, with an initial spin state $\frac{1}{\sqrt{2}}(|+1\rangle + |-1\rangle)$. The cooling of the zero point motion is required to avoid decoherence due to blackbody radiation. This also helps ensure the position and the momentum overlaps are significant. Furthermore, as the particles are coherent states undergoing a series of approximately Gaussian evolutions, with sufficiently precise timings we can ensure a good final overlap is achieved. This zero point motion will also affect the contrast of the interference, known as the Humpty-Dumpty problem [38]. However, the contrast can be made large if the overlap between the position and the momentum of the two trajectories is sufficient, otherwise more repetition in the experimental run will be needed.

The trapping potential is given by $U = (\chi_\rho m B^2/2\mu_0) + mgy$, since $\chi < 0$, the particle can be trapped at a frequency $\omega_\zeta = \sqrt{-(\chi/2\rho\mu_0)(\partial^2 B^2/\partial\zeta^2)}$, where $\zeta = x, y, z$.

A linear magnetic field $\vec{B}_P$ is then pulsed on for a short time relative to the total interferometry time ($t_p \ll T$). This creates a momentum difference correlated with the internal spin state of the particle. The particle then evolves in the weakly trapping potential for some time $t_T$ before the large gradient linear magnetic field is again turned on for a further time $t_P$. At this point, the particle should be returned to its initial position at time $2t_P + t_T \equiv T$, with the internal spin state now in the form $\frac{1}{\sqrt{2}}(e^{i\phi_+}|+1\rangle + e^{-\phi_-}|-1\rangle)$ where the phases $\phi_\pm$ are a result of the interactions with external sources including here, the other interferometer.

To create (and close) the superposition we apply a pulsed magnetic field with the profile

$$\mathbf{B}_p = \eta[y(t=0) - y]\hat{y} + \eta z\hat{z}, \quad (3)$$

where $\eta$ gives the magnetic field gradient and $y(t=0)$ is the initial $y$ position of the particle. We wish to start high in the potential energy curve in the $z$ direction to apply a large momentum difference between the two spin states. With this definition of the pulse field, it makes a minimal disruption to the trapping field, being of zero magnitude (nonzero gradient) at the particle's location [$x = 0$, $y \approx y(t=0)$, and $z \approx 0$].

We control the average magnitude of the induced dipole interaction by initializing the particle in the $y$ direction in a region of large magnetic field. The diamond will then oscillate in the $y$ direction according to the trapping frequency, $\omega_y \sim 10^3$ Hz. This trapping frequency is much faster than that in the splitting ($z$) direction in which the particle is weakly confined (here, $\omega_z \sim 10^2$ Hz). The resulting dual oscillation is seen in Fig. 1(b). See [47] for more information.

To ensure the spatial wave function completely matches at time $t = T$, $\omega_y$ must be an integer multiple of $\omega_z$. It is also necessary that each pulse of the magnetic field matches in both magnitude and pulse time, with deviations leading to reduced contrast in the form of decoherence in the final spin states.

The pulse time $t_p$ is fixed by the magnetic field gradient $\eta$ to maximize the induced momentum difference between the two masses. This requires $t_p/4 = \pi/(2\omega)$, a quarter of the oscillation period, where the frequency is the trapping frequency of the linear magnetic field. Thus $\omega = \sqrt{k/m}$, where $k$ is the spring constant determined by the effective potential of the
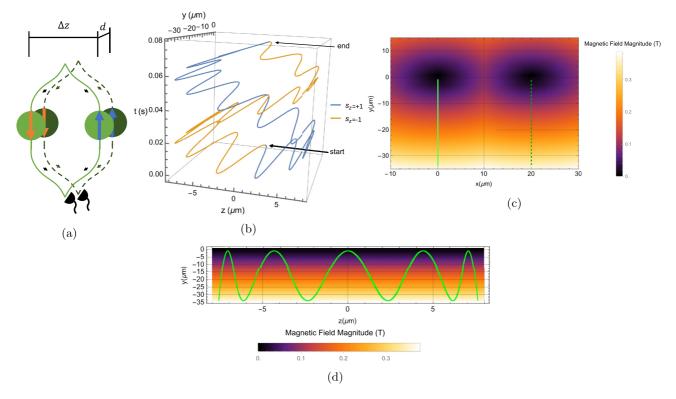
FIG. 1. (a) Schematic representation of the arrangement of the two interferometers, offset by a distance $d$ in the $x$ direction to enable the generation of entanglement. (b) Shows the space-time trajectory for a single interferometer with the $s_z = +1$ state initially oscillating in the positive $z$ direction. (c) The same trajectory in the $x$-$y$ plane showing the interferometer separation distance $d = 20$ μm. (d) Also shows the same trajectory in the $z$-$y$ plane and the trapping magnetic field. Parameters used are $m = 3.8 \times 10^{-19}$ kg, $t_p \approx 160$ μs, and $y(t = 0) = -1.11$ μm.

crystal, $U_{\pm}(y) = -(\chi_{\rho} m/2\mu_0)\eta^2 y^2$, giving

$$t_p = \frac{\pi}{2\eta}\sqrt{\frac{-\mu_0}{2\chi_{\rho}}}, \qquad (4)$$

ensuring that $t_p \ll T$ will simplify the motion as the particle can be treated as receiving a momentum kick from the pulsed magnetic field while oscillating freely in the trapping potential. We here use $t_p \approx 160$ μs $\ll T \approx 0.08$ s which requires $\eta = 10^5$ T m$^{-1}$. More modest magnetic field gradients can also be employed at the cost of a longer pulse time. The ramp sequence used to switch the field on and off with sufficient precision will have to be designed to ensure a good final overlap is achieved.

We can estimate the required precision in the switching times by the zero point motion, which is given by $\delta x \sim \sqrt{\frac{\hbar}{m\omega}} \sim 10^{-9}$ m. Note this is significantly smaller than the interferometer separation and superposition size, so it has a negligible effect on the interaction strength. Given the trapping frequency $\omega_z \sim 10^2$ Hz and the superposition size we propose is $\Delta x \sim 10^{-5}$ m, we require $\frac{\Delta x \omega \delta t}{2\delta x} \ll 1$, giving $\delta t \leqslant 10^{-6}$ s.

The results presented are numerical simulations of the classical equations of motion derived from Eq. (1). The magnetic profile used was $\mathbf{B} = \mathbf{B}_T + \mathbf{B}_p(t)$, where $\mathbf{B}_T$ is given by Eq. (2) and $\mathbf{B}_p(t) = 0$ any time the linear gradient pulse is switched off, otherwise it is given by Eq. (3). Thus, the pulsed magnetic field was taken to be switched on and off instantly.

As shown in Fig. 1(d), due to the downward shift of the rest position of the mass in the background magnetic field due to the downward pull of gravity, the zero-field region of the magnetic field can be avoided by simply initializing the mass away from it. This serves the dual purpose of generating the induced diamagnetic field in the particle and naturally avoiding Majorana spin flips.

Once we have created one superposition in a trapping potential given by Eq. (2), we can imagine bringing two such trapping potentials, hence two interferometers, close to each other at a distance $d$ shown in Fig. 1(a). This gives the parallel setup of the original QGEM proposal, studied in Refs. [3,32,48].

If two such interferometers are placed near one another, separated in the $x$ direction by a distance $d$ with the direction of the spatial splitting parallel as shown in Fig. 1(a), we expect the joint state to evolve to

$$|\Psi\rangle = \frac{1}{2}(|+1, +1\rangle + |-1, -1\rangle)$$
$$+ \frac{e^{i\Delta\phi}}{2}(|+1, -1\rangle + |-1, +1\rangle), \qquad (5)$$

where $\Delta\phi = \phi_{+-} - \phi_{++}$ and $\phi_{ij}$ is the phase due to the interaction between the $i$ and $j$ arms of the interferometer. We refer to this phase difference $\Delta\phi$ as the entanglement phase, which is actually the summation of all particle-particle interactions, considered separately in the following.
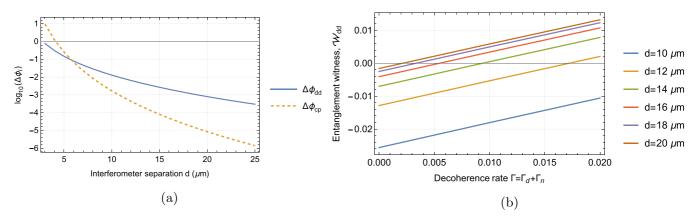
(a)



(b)

FIG. 2. Entanglement phase and witness value comparisons between different signal sources (a) with $\Delta\phi_{DD} > \Delta\phi_{CP}$ for larger separation distances, and as a function of the total decoherent $\Gamma$ (b) showing smaller separation distances yielding more negative results. Here, $m = 3.8 \times 10^{-19}$ kg, $T \approx 0.077$ s, and $t_p \approx 160$ μs.

The use of the Stern-Gerlach effect in generating the superposition leads to the spatially dependent entangling phase being written onto the internal spin degrees of freedom [22]. Therefore, standard NV-center spin readout methods are used to characterize the entanglement.

We are able to experimentally probe various particle-particle interactions mediated by photons by witnessing the entanglement phase. These include Casimir-Polder (CP), and induced dipole-dipole (DD), provided the crystals are neutrally charged [45]. Depending on the chosen experimental parameters, it is likely that at least one of these interactions will be negligible, and indeed, we will consider a situation where only the DD interaction is significant, with the CP interaction serving as the primary background. The potentials for each interaction are

$$U_{CP}(d) = -\frac{23\hbar c}{4\pi} \frac{\varepsilon - 1}{\varepsilon + 2} \frac{\left(\frac{3m}{4\pi\rho}\right)^2}{d^7}, \quad (6)$$

$$U_{DD}(d) = \frac{2\chi_\rho^2 m^2 |\vec{B}(x)|^2}{4\pi\mu_0 d^3}, \quad (7)$$

where $m$, $\rho$, $\chi_\rho$, and $\varepsilon$ are the particle's mass, density, and magnetic mass susceptibility, respectively, and $d$ is the center-of-mass distance between the particles. We consider the magnetic field to be approximately constant across the particles. These interactions $i$ will each give rise to an entanglement phase given by

$$\Delta\phi_i = \frac{1}{\hbar} \int_0^T dt \, U_i[d_1(t)] - U_i[d_2(t)], \quad (8)$$

where $d_1(t)$ [$d_2(t)$] is the furthest (closest) separation distance between the two superposed spatial states.

The entanglement can then be evidenced by measuring an entanglement witness [35], such as

$$\mathcal{W}_i = 1 - \left(2e^{-\frac{1}{2}(\Gamma_n + \Gamma_d)} \sin(\Delta\phi_i) + \frac{1}{2}\left(e^{-2\Gamma_n - \Gamma_d} + 1\right)\right), \quad (9)$$

where $\Gamma_d$ and $\Gamma_n$ are the damping and noise decoherence, respectively. Note that as defined here, this decoherence is defined as the decoherence *rate* multiplied by interferometer time. We plot the witness $\mathcal{W}_{DD}$ with regard to total decoherence and damping: $\Gamma = \Gamma_d + \Gamma_n$ [see Fig. 2(b)]. Entanglement is seen when $\mathcal{W} < 0$ [28]. Figure 2(a) shows how

the entanglement phase from each particle-particle differs with regard to the separation between the two matter-wave interferometers for both the external magnetic field-induced dipole-dipole entanglement and the CP-induced entanglement. We can see that the entanglement witness due to the magnetic dipole-dipole interaction dominates, as expected, at distances $d > 6$ μm [see Fig. 2(b)]. Below this CP-induced entanglement dominates, due to the differing interaction strength scaling with distance $d$. In Fig. 2(b), we have taken the range of decoherence rates and shown that the dominant entanglement is due to the induced magnetic dipole-dipole interaction. Here, we have taken the mass to be similar in both the interferometers, $m = 3.8 \times 10^{-19}$ kg, and the largest superposition we are generating around $\sim$1.1 μm.

We could further modify induced dipole strength, particle charge, mass, and interferometer separation to select optimal regions in which only one interaction dominates. This allows the exploration of the Casimir, dipole, or other interactions independently of one another given their differing dependence on $d$. To gain more precise information about the interactions we need to modify the interaction strength in a controlled fashion. This could involve applying a constant bias magnetic field which would have a negligent effect on the motion, but modify the induced dipole strength, and alternatively slight changes in trap strength, particle mass, or interferometer separation. Each of these will present their own unique challenges in practice.

We should also mention that the time duration of coherence for the NV spin is one of the limiting factors, but the spin coherence times are perpetually increasing (approaching 1s [39], and even 30s [40]), but adapting to our scenario remains an open challenge [49]. We will also have to ensure the external temperature and pressure is below 1 K and $O(10^{-15})$ Pa. We have assumed that the NV spin is not wobbling due to external torque, but in reality, the NV spin will precess, and future analysis has to take this into account [50]. The nanodiamond can also wobble in the presence of the external magnetic field [51]. However, this can be suppressed before being released from the trap by using anisotropically shaped nanoparticles, which can be aligned with any given direction in space by using linearly polarized lasers or electric [51] or magnetic fields [52]. In addition, there will be vibrational

excitations from the breathing mode of the nanodiamond which will also need to be analyzed for this experiment. The phonon vibration can be suppressed for any state manipulation that does not excite the phonons in resonance. It has already been shown that the internal degrees of freedom (phonons) do not pose a problem [53].

To conclude, we have characterized an entanglement for any matter-wave interferometers which relies on creating the macroscopic quantum superposition with the help of a neutral diamagnetic nano-object in the presence of an external magnetic field. We have shown an explicit scheme to create a small-scale spatial superposition to test the known electromagnetic-induced entanglements; the dominant effect arises from external magnetic field-induced dipole-dipole entanglement where the external magnetic field is $O(1)$ T, with a separation of $O(10)$ μm and a mass of $10^{-19}$ kg.

Figures 2(a) and 2(b) show the entanglement is generated via the external magnetic field induced in the nanodiamond, which is essential to create the trapping potential and the superposition. The witness depends on the total decoherence rate and the separation distance $d$. Such a system also allows the characterization of the background effects in gravitational mediated entanglement experiments. Indeed, we have shown how optimizing the distance and trajectories can have a profound effect on the various entangling interactions.

[1] R. Horodecki, P. Horodecki, M. Horodecki, and K. Horodecki, Quantum entanglement, Rev. Mod. Phys. **81**, 865 (2009).

[2] C. H. Bennett, D. P. DiVincenzo, J. A. Smolin, and W. K. Wootters, Mixed-state entanglement and quantum error correction, Phys. Rev. A **54**, 3824 (1996).

[3] P. F. Barker, S. Bose, R. J. Marshman, and A. Mazumdar, Entanglement based tomography to probe new macroscopic forces, Phys. Rev. D **106**, L041901 (2022).

[4] T. W. van de Kamp, R. J. Marshman, S. Bose, and A. Mazumdar, Quantum gravity witness via entanglement of masses: Casimir screening, Phys. Rev. A **102**, 062807 (2020).

[5] H. B. G. Casimir and D. Polder, The influence of retardation on the London–van der Waals forces, Phys. Rev. **73**, 360 (1948).

[6] J. D. Jackson, *Classical Electrodynamics* (Wiley, New York, 1998).

[7] https://www.youtube.com/watch?v=0Fv-0k13s_k (2016), accessed 1 November 2022.

[8] S. Bose, A. Mazumdar, G. W. Morley, H. Ulbricht, M. Toroš, M. Paternostro, A. A. Geraci, P. F. Barker, M. S. Kim, and G. Milburn, Spin entanglement witness for quantum gravity, Phys. Rev. Lett. **119**, 240401 (2017).

[9] C. Marletto and V. Vedral, Gravitationally induced entanglement between two massive particles is sufficient evidence of quantum effects in gravity, Phys. Rev. Lett. **119**, 240402 (2017).

[10] A. Belenchia, R. M. Wald, F. Giacomini, E. Castro-Ruiz, Č. Brukner, and M. Aspelmeyer, Quantum superposition of massive objects and the quantization of gravity, Phys. Rev. D **98**, 126009 (2018).

[11] R. J. Marshman, A. Mazumdar, and S. Bose, Locality and entanglement in table-top testing of the quantum nature of linearized gravity, Phys. Rev. A **101**, 052110 (2020).

[12] S. Bose, A. Mazumdar, M. Schut, and M. Toroš, Mechanism for the quantum natured gravitons to entangle masses, Phys. Rev. D **105**, 106028 (2022).

[13] D. L. Danielson, G. Satishchandran, and R. M. Wald, Gravitationally mediated entanglement: Newtonian field versus gravitons, Phys. Rev. D **105**, 086001 (2022).

[14] M. Christodoulou, A. Di Biagio, M. Aspelmeyer, Č. Brukner, C. Rovelli, and R. Howl, Locally mediated entanglement in linearized quantum gravity, Phys. Rev. Lett. **130**, 100202 (2023).

[15] D. Biswas, S. Bose, A. Mazumdar, and M. Toroš, Gravitational optomechanics: Photon-matter entanglement via graviton exchange, Phys. Rev. D **108**, 064023 (2023).

[16] B. Yi, U. Sinha, D. Home, A. Mazumdar, and S. Bose, Massive spatial qubits: Testing macroscopic nonclassicality and Casimir entanglement, Phys. Rev. Res. **5**, 033202 (2023).

[17] M. Bloom and K. Erdman, The transverse Stern–Gerlach experiment, Can. J. Phys. **40**, 179 (1962).

[18] S. Machluf, Y. Japha, and R. Folman, Coherent Stern–Gerlach momentum splitting on an atom chip, Nat. Commun. **4**, 2424 (2013).

[19] O. Amit, Y. Margalit, O. Dobkowski, Z. Zhou, Y. Japha, M. Zimmermann, M. A. Efremov, F. A. Narducci, E. M. Rasel, W. P. Schleich, and R. Folman, $T^3$ Stern-Gerlach matter-wave interferometer, Phys. Rev. Lett. **123**, 083601 (2019).

[20] Y. Margalit, O. Dobkowski, Z. Zhou, O. Amit, Y. Japha, S. Moukouri, D. Rohrlich, A. Mazumdar, S. Bose, C. Henkel, and R. Folman, Realization of a complete Stern-Gerlach interferometer: Toward a test of quantum gravity, Sci. Adv. **7**, eabg2879 (2021).

[21] C. Wan, M. Scala, G. W. Morley, ATM. A. Rahman, H. Ulbricht, J. Bateman, P. F. Barker, S. Bose, and M. S. Kim, Free nano-object Ramsey interferometry for large quantum superpositions, Phys. Rev. Lett. **117**, 143003 (2016).

[22] M. Scala, M. S. Kim, G. W. Morley, P. F. Barker, and S. Bose, Matter-wave interferometry of a levitated thermal nano-oscillator induced and probed by a spin, Phys. Rev. Lett. **111**, 180403 (2013).

[23] J. S. Pedernales, G. W. Morley, and M. B. Plenio, Motional dynamical decoupling for interferometry with macroscopic particles, Phys. Rev. Lett. **125**, 023602 (2020).

[24] R. J. Marshman, A. Mazumdar, R. Folman, and S. Bose, Constructing nano-object quantum superpositions with a Stern-Gerlach interferometer, Phys. Rev. Res. **4**, 023087 (2022).

[25] R. Zhou, R. J. Marshman, S. Bose, and A. Mazumdar, Catapulting towards massive and large spatial quantum superposition, Phys. Rev. Res. **4**, 043157 (2022).

[26] R. Zhou, R. J. Marshman, S. Bose, and A. Mazumdar, Mass-independent scheme for enhancing spatial quantum superpositions, Phys. Rev. A **107**, 032212 (2023).

[27] R. Zhou, R. J. Marshman, S. Bose, and A. Mazumdar, Gravito-diamagnetic forces for mass independent large spatial quantum superpositions, arXiv:2211.08435.

[28] H. Chevalier, A. J. Paige, and M. S. Kim, Witnessing the nonclassical nature of gravity in the presence of unknown interactions, Phys. Rev. A **102**, 022428 (2020).

[29] O. Romero-Isart, M. L. Juan, R. Quidant, and J. I. Cirac, Toward quantum superposition of living organisms, New J. Phys. **12**, 033015 (2010).

[30] O. Romero-Isart, Quantum superposition of massive objects and collapse models, Phys. Rev. A **84**, 052121 (2011).

[31] O. Romero-Isart, A. C. Pflanzer, F. Blaser, R. Kaltenbaek, N. Kiesel, M. Aspelmeyer, and J. I. Cirac, Large quantum superpositions and interference of massive nanometer-sized objects, Phys. Rev. Lett. **107**, 020405 (2011).

[32] H. C. Nguyen and F. Bernards, Entanglement dynamics of two mesoscopic objects with gravitational interaction, Eur. Phys. J. D **74**, 1 (2020).

[33] A. Bassi, K. Lochan, S. Satin, T. P. Singh, and H. Ulbricht, Models of wave-function collapse, underlying theories, and experimental tests, Rev. Mod. Phys. **85**, 471 (2013).

[34] M. Schut, J. Tilly, R. J. Marshman, S. Bose, and A. Mazumdar, Improving resilience of quantum-gravity-induced entanglement of masses to decoherence using three superpositions, Phys. Rev. A **105**, 032411 (2022).

[35] M. Toroš, T. W. van de Kamp, R. J. Marshman, M. S. Kim, A. Mazumdar, and S. Bose, Relative acceleration noise mitigation for nanocrystal matter-wave interferometry: Applications to entangling masses via quantum gravity, Phys. Rev. Res. **3**, 023178 (2021).

[36] D. Fitzakerley, M. George, E. Hessels, T. Skinner, C. Storry, M. Weel, G. Gabrielse, C. Hamley, N. Jones, K. Marable *et al.*, Electron-cooled accumulation of $4 \times 10^9$ positrons for production and storage of antihydrogen atoms, J. Phys. B: At., Mol. Opt. Phys. **49**, 064001 (2016).

[37] A. Marx, J. Hoess, and K. Uhlig, Dry dilution refrigerator for experiments on quantum effects in the microwave regime, arXiv:1412.3619.

[38] J. Schwinger, M. O. Scully, and B. G. Englert, Is spin coherence like Humpty-Dumpty? Z. Phys. D: At., Mol. Clusters **10**, 135 (1988).

[39] N. Bar-Gill, L. M. Pham, A. Jarmola, D. Budker, and R. L. Walsworth, Solid-state electronic spin coherence time approaching one second, Nat. Commun. **4**, 1743 (2013).

[40] M. H. Abobeih, J. Cramer, M. A. Bakker, N. Kalb, M. Markham, D. J. Twitchen, and T. H. Taminiau, One-second coherence for a single electron spin coupled to a multi-qubit nuclear-spin environment, Nat. Commun. **9**, 2552 (2018).

[41] J. T. Muhonen, J. P. Dehollain, A. Laucht, F. E. Hudson, R. Kalra, T. Sekiguchi, K. M. Itoh, D. N. Jamieson, J. C. McCallum, A. S. Dzurak, and A. Morello, Storing quantum information for 30 seconds in a nanoelectronic device, Nat. Nanotechnol. **9**, 986 (2014).

[42] D. Farfurnik, A. Jarmola, L. M. Pham, Z. H. Wang, V. V. Dobrovitski, R. L. Walsworth, D. Budker, and N. Bar-Gill, Optimizing a dynamical decoupling protocol for solid-state electronic spin ensembles in diamond, Phys. Rev. B **92**, 060301(R) (2015).

[43] M.-Z. Wu, M. Toroš, S. Bose, and A. Mazumdar, Quantum gravitational sensor for space debris, Phys. Rev. D **107**, 104053 (2023).

[44] M. Toroš, A. Mazumdar, and S. Bose, Loss of coherence of matter-wave interferometer from fluctuating graviton bath, arXiv:2008.08609.

[45] M. Frimmer, K. Luszcz, S. Ferreiro, V. Jain, E. Hebestreit, and L. Novotny, Controlling the net charge on a nanoparticle optically levitated in vacuum, Phys. Rev. A **95**, 061801(R) (2017).

[46] J.-F. Hsu, P. Ji, C. W. Lewandowski, and B. D'Urso, Cooling the motion of diamond nanocrystals in a magneto-gravitational trap in high vacuum, Sci. Rep. **6**, 30125 (2016).

[47] See Supplemental Material at http://link.aps.org/supplemental/10.1103/PhysRevA.109.L030401 for more information on the equations of motion of the particles and trajectory through the magnetic potential.

[48] J. Tilly, R. J. Marshman, A. Mazumdar, and S. Bose, Qudits for witnessing quantum-gravity-induced entanglement of masses under decoherence, Phys. Rev. A **104**, 052416 (2021).

[49] B. D. Wood, G. A. Stimpson, J. E. March, Y. N. D. Lekhai, C. J. Stephen, B. L. Green, A. C. Frangeskou, L. Ginés, S. Mandal, O. A. Williams, and G. W. Morley, Long spin coherence times of nitrogen vacancy centers in milled nanodiamonds, Phys. Rev. B **105**, 205401 (2022).

[50] Y. Japha and R. Folman, Quantum uncertainty limit for Stern-Gerlach interferometry with massive objects, Phys. Rev. Lett. **130**, 113602 (2023).

[51] B. A. Stickler, K. Hornberger, and M. S. Kim, Quantum rotations of nanoparticles, Nat. Rev. Phys. **3**, 589 (2021).

[52] A. A. Wood, R. M. Goldblatt, R. E. Scholten, and A. M. Martin, Quantum control of nuclear-spin qubits in a rapidly rotating diamond, Phys. Rev. Res. **3**, 043174 (2021).

[53] C. Henkel and R. Folman, Internal decoherence in nano-object interferometry due to phonons, AVS Quantum Sci. **4**, 025602 (2022).